Available online at www.sciencedirect.com
ScienceDirect
Earth and Planetary Science Letters 260 (2007) 313–327
EPSL
www.elsevier.com/locate/epsl

Shortening of analogue models with contractive substrata: Insights into the origin of purely landward-vergent thrusting wedge along the Cascadia subduction zone and the deformation evolution of Himalayan–Tibetan orogen

Jianxun Zhou [a,*], Fengyin Xu [b], Chunguang Wei [a], Gang Li [a], Fusheng Yu [a], Hengmao Tong [a]

[a] *Department of Earth Science, China University of Petroleum, Beijing 102249, PR China*
[b] *Qinghai Petroleum Sub-corporation of PetroChina Company Limited, Dunhuang 736202, PR China*

Received 12 September 2006; received in revised form 22 May 2007; accepted 23 May 2007
Available online 2 June 2007
Editor: R.D. van der Hilst

Abstract

Origin of certain uncommon fold-and-thrust belts, such as the purely landward-vergent (rearward-vergent) thrusting wedge along the Cascadia subduction zone and the wide flat-toped Himalayan–Tibetan orogen, were proposed to be closely related to their ductile substrata. Results of a series of sandbox models with contractive substrata of various contracting velocities and different contracting directions, designed to study the influences of horizontal contraction of ductile substrata on deformation evolution and structural style of fold-and-thrust belts, show that purely rearward-vergent thrusting wedges can be reproduced under the condition of syn-directionally horizontal contraction of the ductile substrata, without other requirements of forward-dipping backstops, landward dipping detachments and strong wedges relative to weak bases. Therefore syn-directionally horizontal contraction of the ductile substrata can be considered an important cause for the formation of purely landward-vergent thrusting wedge along the Cascadia subduction zone. Our modeling results, together with the results of some other previous physical and numerical models, reinforce the opinion that the deformation evolution of the Himalayan–Tibetan orogen were likely governed by its weak lower crust and suggest that the north and south edges of the Himalayan–Tibetan orogen may have undergone almost synchronous Cenozoic deformation evolution owing to the existence of weak lower crust. It is also proposed that: (1) development of thrusts in the Himalayan–Tibetan orogen may not necessarily occur in a frontward sequence; (2) much later uplift deduced from Cenozoic sedimentary records in the basins along the northeastern margin of the Himalayan–Tibetan orogen does not necessarily imply much later initiation of uplift and deformation at the northeastern margin of the orogen.

Keywords: physical modelling; landward-vergent thrusting; Cascadia subduction zone; Himalayan–Tibetan orogen; deformation mechanism

* Corresponding author. Tel.: +86 10 889741163; fax: +86 10 89733291.
E-mail address: jxzhou@bjpeu.edu.cn (J. Zhou).

0012-821X/$ - see front matter © 2007 Published by Elsevier B.V.
doi:10.1016/j.epsl.2007.05.048

1. Introduction

Crustal shortening is the most common deformation form mainly taking place along convergent plate boundaries and generally results in the formation of fold-and-thrust belts or accretionary wedges. Investigations based on the Mohr–Coulomb critical wedge theory and physical modeling experiments have indicated that structural styles of fold-and-thrust belts have been influenced by various factors, such as thickness and strength of strata (Davis et al., 1983; Dahlen, 1990; Liu et al., 1992; Lohrmann et al., 2003; Teixell and Koyi, 2003), pore fluid pressure (Cobbold et al., 2001), geometry and strength of backstop (Byrne et al., 1993; Lallemand et al., 1994; Bonini et al., 2000; Rossetti et al., 2002), shear-strength and dip of basal detachment (Davis et al., 1983; Dahlen, 1990; Liu et al., 1992; Koyi and Vendeville, 2003; Smit et al., 2003), synchronous sedimentation or erosion (Storti and McClay, 1995; Mugnier et al., 1997; Persson and Sokoutis, 2002), sediment underplating (Gutscher et al., 1998), and surface slope and topography (Marques and Cobbold, 2002, 2006). It has been revealed by physical modeling experiments (e.g. Liu et al., 1992; Cotton and Koyi, 2000; Costa and Vendeville, 2002; Lujan et al., 2003) that among above factors, shear-strength of basal detachment may have played a crucial role in the deformation evolution and structural style of fold-and-thrust belts. Lower shear-strength of basal detachment usually results in a wider fold-and-thrust belt of lower taper and dual vergence, i.e., of both forward (or seaward) and rearward (or landward) vergence, whereas higher shear-strength of basal detachment normally produces narrower fold-and-thrust belts of higher taper predominated by forward-vergent thrusts (Liu et al., 1992; Cotton and Koyi, 2000; Costa and Vendeville, 2002; Lujan et al., 2003). Some uncommon fold-and-thrust belts in nature, such as the purely landward-vergent thrusting wedge along the Cascadia subduction zone and the wide Himalayan–Tibetan orogen characterized by flat-top and steep-side, were proposed to be closely related to the existence of ductile substrata, generally regarded as the major cause of lower shear-strength basal detachment. For the purely landward-vergent thrusting wedge along the Cascadia subduction zone the ductile substratum is considered to be composed of calcareous mudstone probably with excess pore-fluid pressure (Gutscher et al., 2001), while for the Himalayan–Tibetan orogen its weak lower crust has been regarded as the ductile substratum (Zhao and Morgan, 1987; Bird, 1991; Royden et al., 1997; Owens and Zandt, 1997; Clark and Royden, 2000; Shen et al., 2001; Beaumont et al., 2001; DeCelles et al., 2002; Beaumont et al., 2004).

Recently, physical modeling experiments have been increasingly employed to investigate the influences of ductile substrata on the deformation evolution and structural style of fold-and-thrust belts (e.g. Bonini et al., 2000; Cotton and Koyi, 2000; Rossetti et al., 2000; Gutscher et al., 2001; Rossetti et al., 2002; Costa and Vendeville, 2002; Smit et al., 2003; Lujan et al., 2003; Couzens-Schultz et al., 2003; Bonini, 2003). The experimental results, however, often exhibit apparently different structural styles, largely because of differences

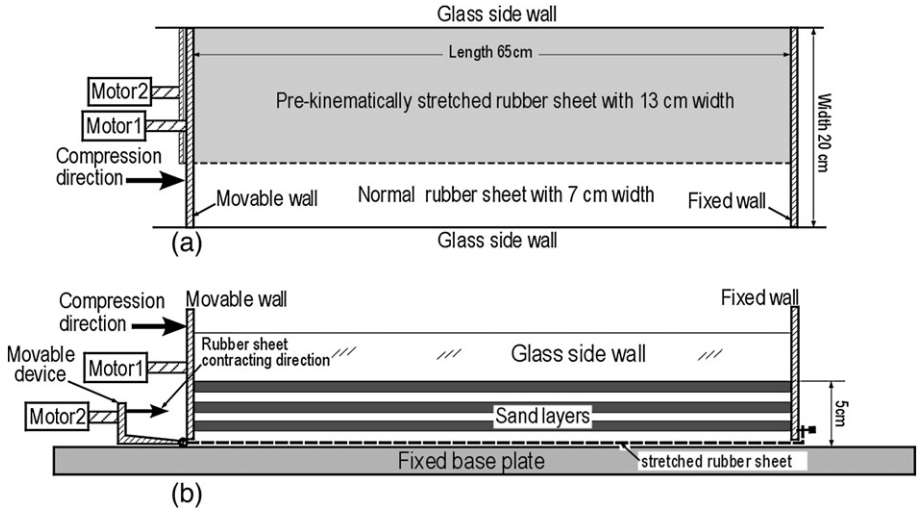

Fig. 1. Schematic illustration of configurations of the model with syn-directionally contracted substratum: (a) plan view of the model configuration showing the wider half with contractive substratum and the narrower half with frictional substratum, (b) cross-sectional view of the wider half with contractive substratum.

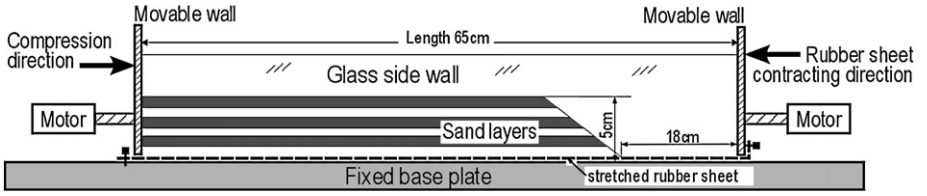

Fig. 2. Schematic cross-sectional illustration of configurations of the model with anti-directionally contracted substratum.

in substratum thickness, viscosity and strain rate, which are the three governing parameters of the shear-strength of ductile substrata (Costa and Vendeville, 2002; Bonini, 2003). Ductile substrata in most previous experiments often deformed in complex fashions, i.e., not only asymmetric cumulative advection, but also flowing upwards or even diapirically, and the fold-and-thrust belts were predominated by the structural style of dual (both forward- and rearward-) vergent thrusting (Cotton and Koyi, 2000; Costa and Vendeville, 2002; Smit et al., 2003; Lujan et al., 2003; Couzens-Schultz et al., 2003; Bonini, 2003). Unfortunately, from the previous experiments we can not easily identify the detailed effects of each deformation fashions in ductile substrata, although it is certain that the deformation of the fold-and-thrust belts must be complexly influenced by all these deformation fashions of the ductile substrata.

In the physical models of Gutscher et al. (2001) with ductile substrata of silicone putty, the structural style of purely landward-vergent thrusting was successfully reproduced only at a moderate convergence rate of 0.5–1 cm/min. The fact that the silicone putty layer did not show obvious upward flow, however, does imply that the ductile substrata of their physical models may have only undergone asymmetric cumulative advection. On the other hand, the influences of weak lower crust flow on the Cenozoic upper-crustal deformation of the Himalayan–Tibetan orogen were studied mainly by numerical modeling experiments of mechanical or thermal-mechanical models (Zhao and Morgan, 1987; Bird, 1991; Royden et al., 1997; Clark and Royden, 2000; Shen et al., 2001; Beaumont et al., 2001; Beaumont et al., 2004). Although physical modeling experiments have been used to study the tectonic problems of the Himalayan–Tibetan orogen for a long time (e.g. Tapponnier et al., 1982; Peltzer and Tapponier, 1988; Burg et al., 1994; Chemenda et al., 1995; Dubey, 1997; Chemenda et al., 2000; Sokoutis et al., 2000), there is still a lack of such experiments on the influences of weak lower crust flow.

In this paper, we present results of a series of sandbox modeling experiments with contractive substrata of various contracting velocities and different contracting directions to study the influences of horizontal contraction of ductile substrata on deformation evolution and structural style of fold-and-thrust belts. Our physical models with contractive substrata also successfully reproduced the structural style of purely landward-vergent thrusting as did the physical models of Gutscher et al. (2001). These physical modeling experiments

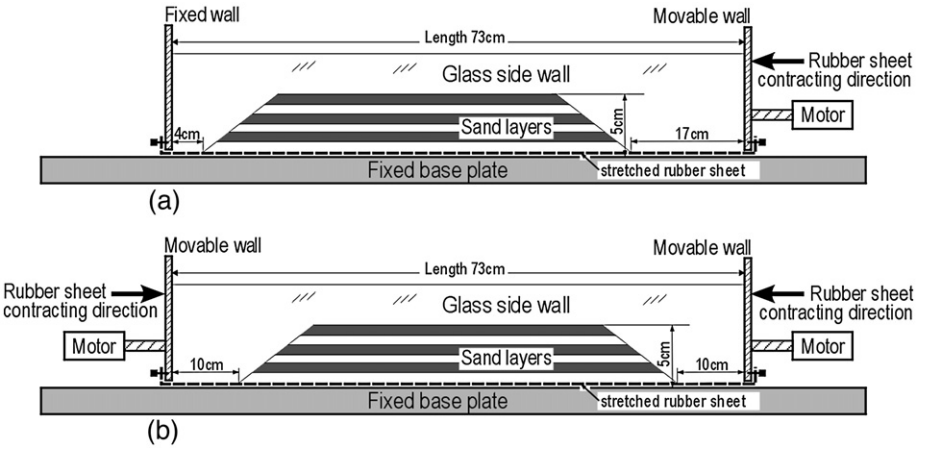

Fig. 3. Schematic cross-sectional illustration of configurations of the models with contracted substratum but without compression from rear wall: (a) the model with asymmetrically contracted substratum, (b) the model with symmetrically contracted substratum.

provide insights on the origin of purely landward-vergent thrusting wedge along the Cascadia subduction zone and also on the deformation evolution of the Himalayan–Tibetan orogen, which we will discuss in some detail hereinafter.

2. Model construction

A sandbox rig with a width of 20 cm was used in our experiments. The base of all models was horizontal and planar, and laid by a rubber sheet of a thickness of 2 mm, which was then overlaid by sand layers of various colors. Three kinds of models with contractive substrata were involved in this study.

In the model with syn-directionally contracted substratum (i.e., the contracting direction is the same as the compression direction), the rubber sheet was cut along the compression direction into two halves with widths of 7 cm and 13 cm, respectively (Fig. 1a). The rubber sheet of the narrower half had a length of 65 cm and was affixed to the base of model. The rubber sheet of the wider half had an initial length of 50 cm, whose one end was attached to the bottom of the fixed wall and the other end was connected to a movable device driven by Motor 2 (Fig. 1b). It was then pre-kinematically stretched to 65 cm (equal to the length of the narrower half) before sand layers were put on. The model was compressed by a displacement of 15 cm from the movable wall driven by Motor 1 at a constant displacement velocity of 4.40×10^{-3} cm/s, while the movable device driven by Motor 2 contracted the pre-kinematically stretched rubber sheet in the same direction at various displacement velocities to simulate the syn-

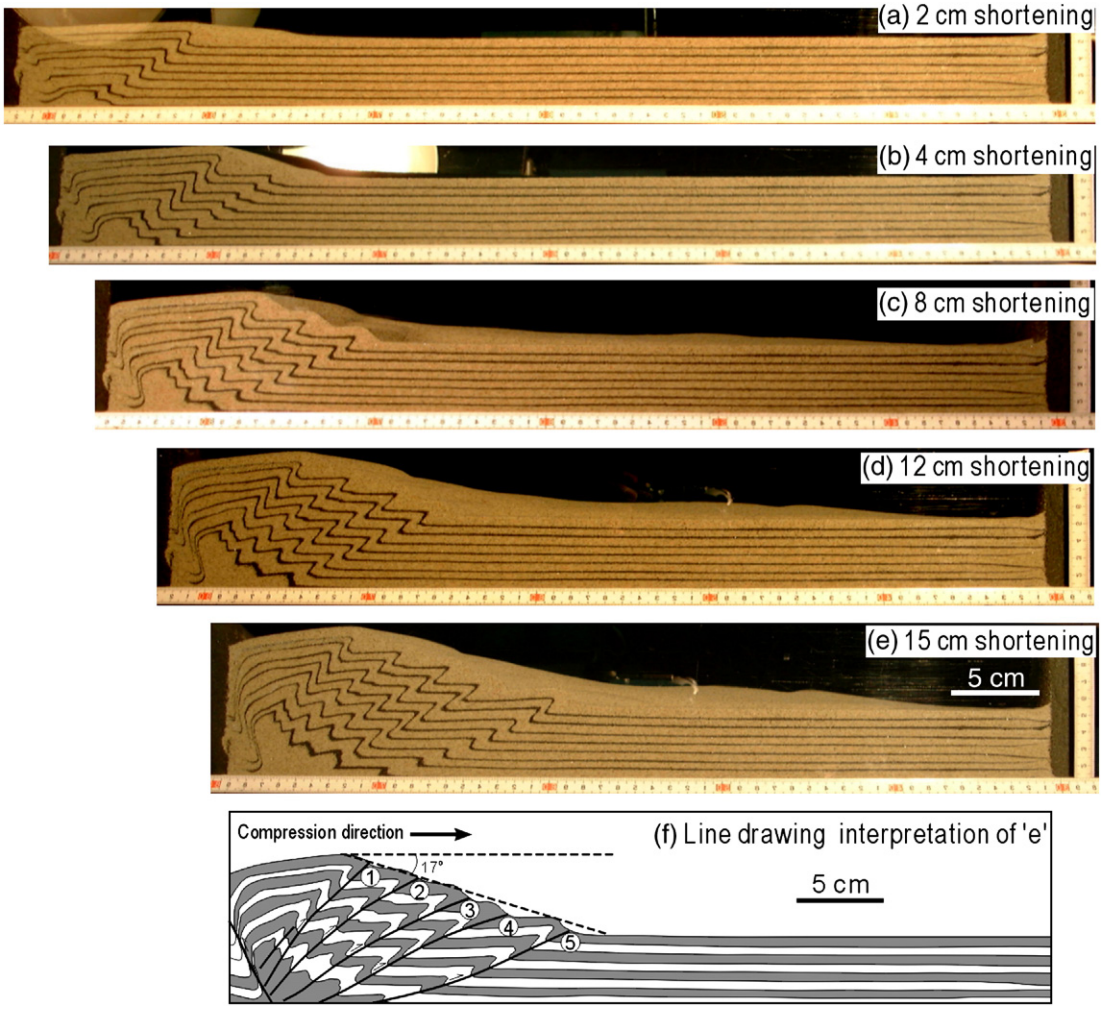

Fig. 4. The sequential photographs show evolution of the forward-vergent thrusting wedge above the frictional substratum of the model. The movable wall of the model displaced at a constant velocity of 4.40×10^{-3} cm/s. Numbering in (f) indicates the sequences of thrusts.

directionally horizontal contraction of ductile substratum. The substratum of pre-kinematically stretched rubber sheet in the three representative models presented in this paper was contracted, driven by Motor 2, at a displacement velocity of 4.40×10^{-3} cm/s, 2.93×10^{-3} cm/s and 1.47×10^{-3} cm/s respectively, which are equal to, two thirds of and one third of that of the movable wall, respectively. Consequently, all models deformed above two types of substrata, i.e., the wider half above ductile substratum of syn-directionally horizontal contraction and the narrower half above frictional substratum, both under same other conditions. The merit of such setting is that we can easily compare the deformation features above two types of substrata in the same experiment.

In the model with anti-directionally contracted substratum (i.e., the contracting direction is opposite to the compression direction), the rubber sheet with a width of 20 cm had an initial length of 50 cm, whose one end was attached to the bottom of the right movable wall and the other end was fixed on the base plate of the sandbox rig (Fig. 2). It was then pre-kinematically stretched to 65 cm before sand layers were put on. The right end of sand layers had a free slope and a safety distance to the right movable wall to prevent compression (Fig. 2). The model was compressed with a displacement of 13 cm from left movable wall at a constant displacement velocity of 4.40×10^{-3} cm/s, while the pre-kinematically stretched rubber sheet was simultaneously contracted by right movable wall from the opposite direction with same displacement at identical displacement velocity.

In the models with contracted substratum but without compression from rear walls, the rubber sheets had a

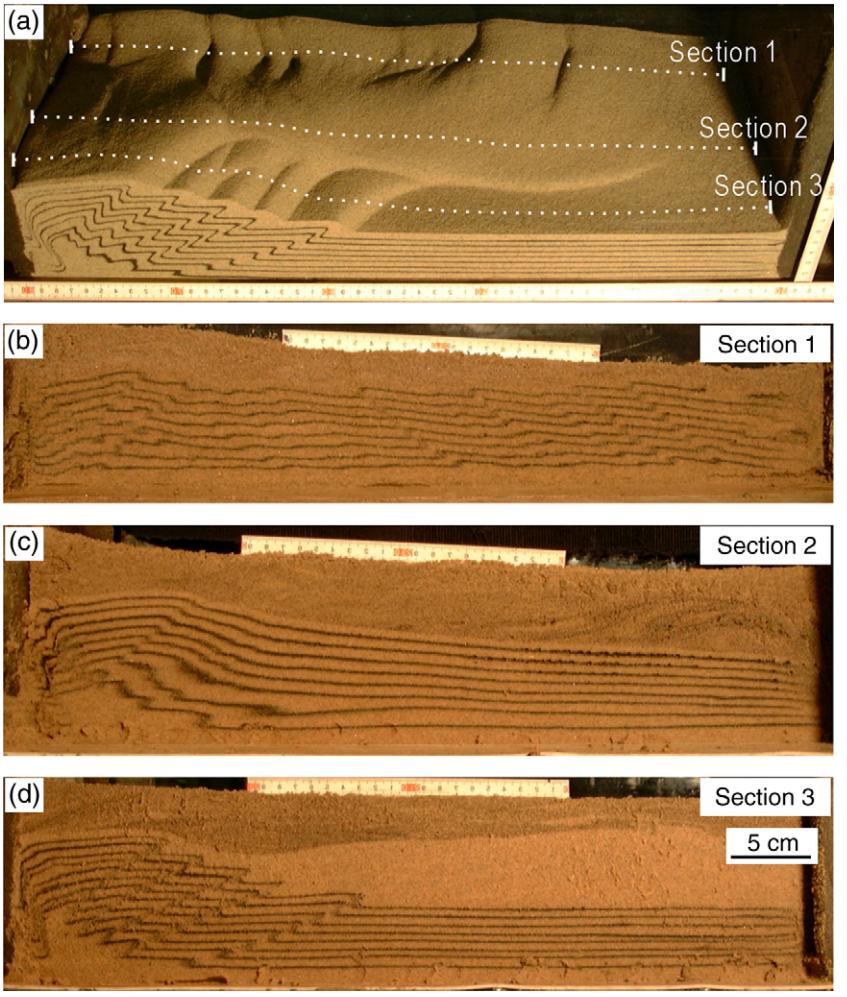

Fig. 5. The 3-D view and three inner sections cut parallel to shortening direction show the surface deformation features and inner structural styles of the two halves of the model respectively above frictional substratum and contractive substratum after 15 cm of shortening. The contraction of the substratum and the displacement of the movable wall are equal at a constant velocity of 4.40×10^{-3} cm/s.

width of 20 cm and an initial length of 53 cm, whose ends were attached to the bottom of movable or fixed walls (Fig. 3). It was then pre-kinematically stretched to 73 cm before sand layers were put on. The sand layers had free end slopes and safety distances to the movable or fixed walls to prevent compression (Fig. 3). Therefore, the models were deformed only by contracted substratum and without compression from rear walls. In the model with asymmetrically contracted substratum (Fig. 3a), the rubber sheet was contracted from one direction at a constant displacement velocity of 4.40×10^{-3} cm/s with a displacement of 15 cm; while in the model with symmetrically contracted substratum (Fig. 3b), the rubber sheet was simultaneously contracted from two opposite directions both at a constant displacement velocity of 2.20×10^{-3} cm/s with a displacement of 7.5 cm, hence with a total contraction of 15 cm.

All experiments were conducted in the Tectonophysics Laboratory at China University of Petroleum in Beijing. Dry, 0.2–0.3 mm grain size quartz sand, which has an inner frictional angle of 30°–31°, was used to simulate the brittle upper crust. Dry quartz sand has long been recognized as an appropriate analogue material for simulating brittle deformation in the upper crust due to its nearly perfect Mohr–Coulomb behavior (Davy and Cobbold, 1991). The sand layers in all models have an initial total thickness of 5 cm and are interlaid by thin layers of the same sand colored by black ink. The frictional coefficient between sand layers and the normal (i.e. non-contracted) rubber sheets is ~0.49. The glass side walls were carefully cleaned to reduce the influence

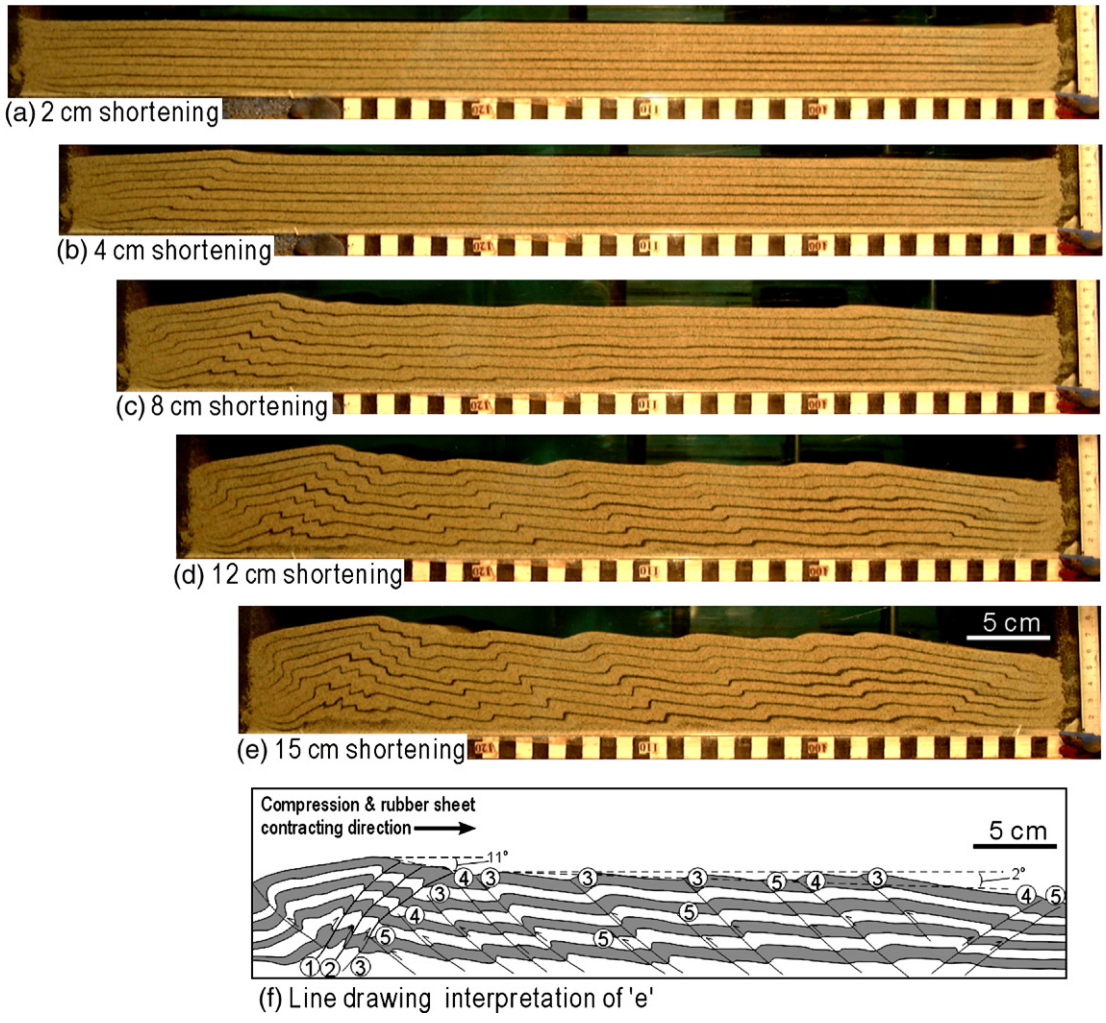

Fig. 6. The sequential photographs show deformation evolution of the wider half model above contractive substratum syn-directionally contracted at a constant velocity of 4.40×10^{-3} cm/s, equal to the displacement velocity of the movable wall. Numbering in (f) indicates the sequences of thrusts.

from lateral friction. The side and top views of each model were photographed at fixed displacement intervals. After shortening, the models were covered by sand, then wetted and sectioned to examine the along-strike variations of deformation features. All models were repeated at least twice and similar results were obtained. To benefit comparison of deformation features between the opposite sides of models, some photos from one side are horizontally flipped to show the same compression direction with those from the other side.

3. Experimental results

3.1. Model with syn-directionally contracted substratum

Like other previous physical models of frictional substrata (e.g. Liu et al., 1992; Cotton and Koyi, 2000; Lujan et al., 2003), deformation in the narrower half of our physical model above frictional substratum initiated with the formation of a box fold, a forward-vergent thrust and a rearward-vergent thrust at the front of movable wall (Fig. 4a). Continued shortening progressively formed a forward-vergent thrusting wedge in a frontward sequence, and caused back-rotation of the older thrust sheets and gradual increase in dips of the older forward-vergent thrusts, whereas initial dips of the younger forward-vergent thrusts gradually decreased from ~32° to ~25° (Fig. 4b–e). As shortening reached 15 cm, a forward-vergent thrusting wedge of ~17° taper formed (Fig. 4f). The inner section cut parallel to shortening direction (Fig. 5d) shows same deformation pattern with that observed from the glass side wall (Fig. 4e).

Deformation pattern in the wider half of the model (Fig. 5b) above contractive substratum that was contracted syn-directionally at a constant velocity of 4.40×10^{-3} cm/s (equal to the displacement velocity of the movable wall) distinctly differs from that in the narrower half of the model (Fig. 5d) above frictional substratum. The deformation above the syn-directionally contracted substratum was more distributed and propagated obviously faster and farther than that above the frictional substratum. Apparently there existed a transpressive accommodation zone subparallel to the compression direction between the two halves of the model (Fig. 5a). During early shortening stages, visible thrusts above the syn-directionally contracted substratum initiated obviously later than those above the frictional substratum (compare Fig. 6a with 4a). After 4 cm of shortening, a box fold with a distinct forward-vergent thrust initiated at the front of the movable wall (Fig. 6b). With continuous shortening, more forward-vergent thrusts progressively developed in a frontward sequence with initial dips of ~37°, which composed a higher-taper forward-vergent thrusting domain. After 8 cm of shortening, a series of visible rearward-vergent thrusts synchronously developed with initial dips of ~38° and composed a lower-taper purely rearward-vergent thrusting domain juxtaposed against the higher-taper forward-vergent thrusting domain (Fig. 6c). Progressive deformation obviously increased the displacements and numbers of the rearward-vergent thrusts and slightly increased (~3°) the dips of the rearward-vergent thrusts in the lower-taper purely rearward-vergent thrusting domain, and formed two forward-vergent thrusts in the toe of the purely rearward-vergent thrusting domain. However, the numbers of forward-vergent thrusts in the

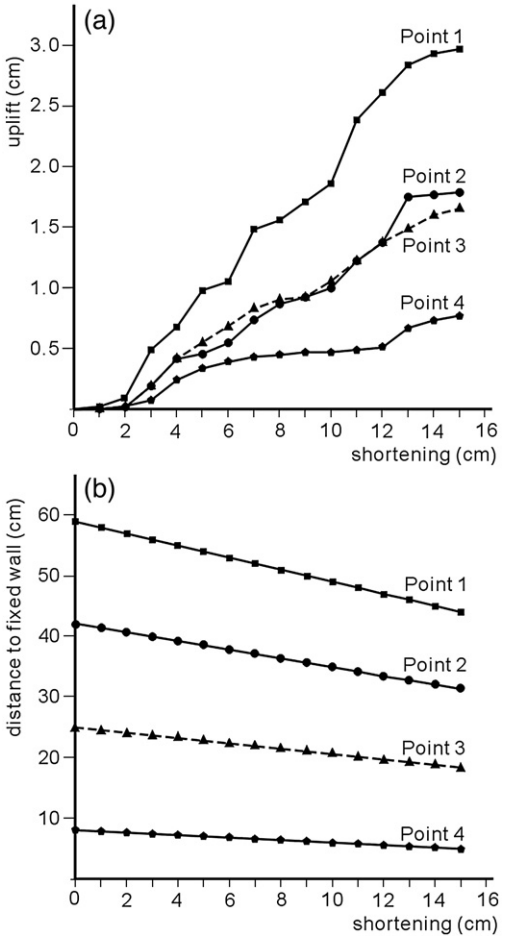

Fig. 7. Plots of uplift versus shortening (a) and plots of distance to fixed wall versus shortening (b) of four reference points on the surface of the wider half above contractive substratum contracted at a constant velocity of 4.40×10^{-3} cm/s, equal to the displacement velocity of the movable wall. The initial distance between the fixed wall and Points 1, 2, 3 and 4 was 59, 42, 25 and 8 cm, respectively.

higher-taper forward-vergent thrusting domain almost kept constant, but their dips increased obviously with an increment of ~10° (Fig. 6d–e).

After 15 cm of shortening, the higher-taper forward-vergent thrusting domain exhibited a taper of ~11° (Fig. 6f), which is distinctly lower than that in the model above frictional substratum (Fig. 4f). The purely rearward-vergent thrusting domain has a nearly horizontal surface and an average taper of ~2° (Fig. 6f). The inner section cut parallel to shortening direction in the half model above contractive substratum (Fig. 5b) also shows identical structural style with that observed from the glass side wall (Fig. 6e), indicating that structural styles observed from glass side walls of the models were not markedly influenced by lateral friction and therefore can be effectively used for discussion on deformation of the models. The inner section cut along the transpressive accommodation zone between the two halves of the model shows predominantly distributed deformation with merely a few thrusts at its rear (Fig. 5c).

The variations in elevation and displacement relative to the fixed wall of a series of reference points on the surface of the wider half model above contractive substratum were measured and the representative results of four reference points are presented by the plots of uplift versus shortening (Fig. 7a) and the plots of distance to the fixed wall versus shortening (Fig. 7b). Initial distances of the four reference points to the fixed wall were 59, 42, 25 and 8 cm, respectively. All the plots of uplift versus shortening exhibited rough flat-ramp shapes and similar trends, but with notable differences (Fig. 7a), while all the plots of distance to the fixed wall versus shortening show basically linear shape (Fig. 7b). Uplift of the all reference points is approximately in direct proportion to the shortening of model and apparently faster on the rear of the model than on the front of the model (Fig. 7a). Moreover, visible initial uplift at the front of the model (see Point 4 in Fig. 7a) is slightly later than that at the rear of the model (see Point 1 in Fig. 7a) and perturbations of the plots of uplift versus shortening gradually weaken from the rear of the model to the front of the model (Fig. 7a, from Point 1 to Point 4), whereas the reference points in the central purely rearward-vergent thrusting domain show very similar uplift paths (Fig. 7a, Point 2 and Point 3).

As the substrata contracting velocities increased, deformation features in the wider halves of the models above contractive substratum gradually changed, with the deformation more distributed, the taper of the forward-vergent thrusting domains lower and the purely rearward-vergent thrusting domains more distinctive (Fig. 8a–d). When the substratum contracting velocity was only 1.47×10^{-3} cm/s (only one third of the displacement

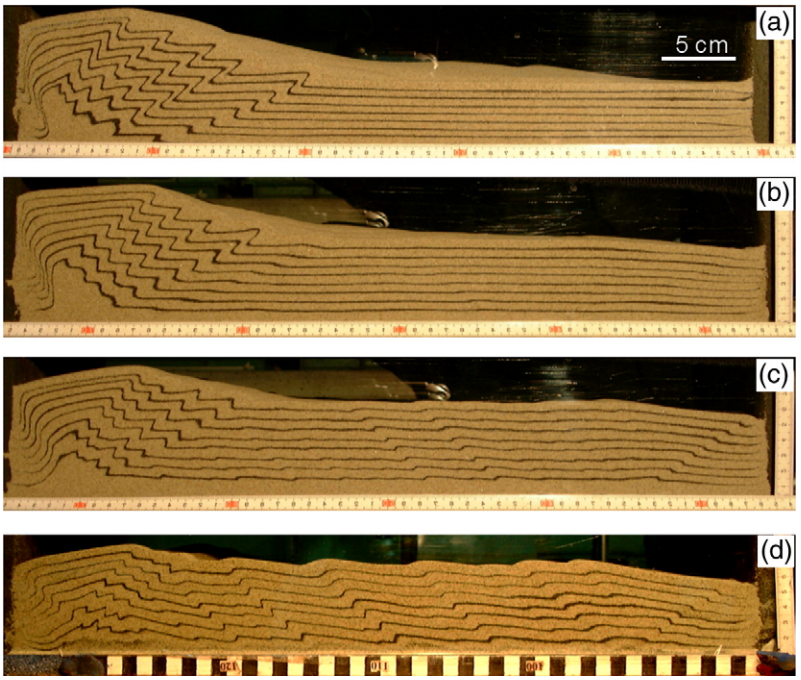

Fig. 8. Comparison of deformation styles among the models with different substrata situations after 15 cm of shortening. (a) Frictional substratum. (b), (c) and (d) contractive substratum, respectively contracted at different velocity of 1.47×10^{-3} cm/s, 2.93×10^{-3} cm/s and 4.40×10^{-3} cm/s.

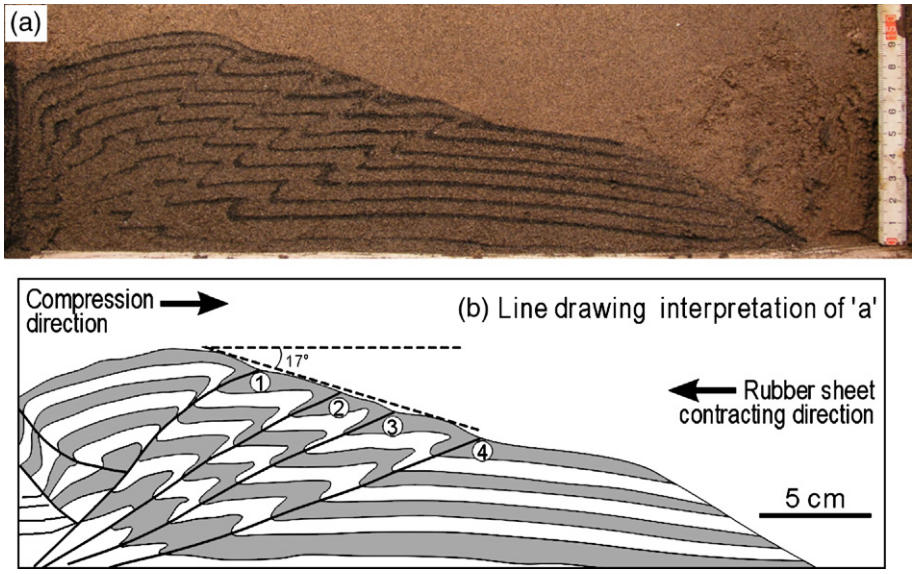

Fig. 9. The photograph of an inner section cut parallel to shortening direction of the model with anti-directionally contracted substratum (a) and its interpretation (b). The model was compressed and its substratum was simultaneously contracted from the opposite direction both at the constant displacement velocity of 4.40×10^{-3} cm/s with a displacement of 13 cm. Numbering in (b) indicates the sequences of thrusts.

velocity of the movable wall), the rearward-vergent thrusts were visible even at early stages of deformation (Fig. 8b), indicating that even small degree of syn-directionally horizontal contraction of substratum may also favor the formation of purely rearward-vergent thrusting domains.

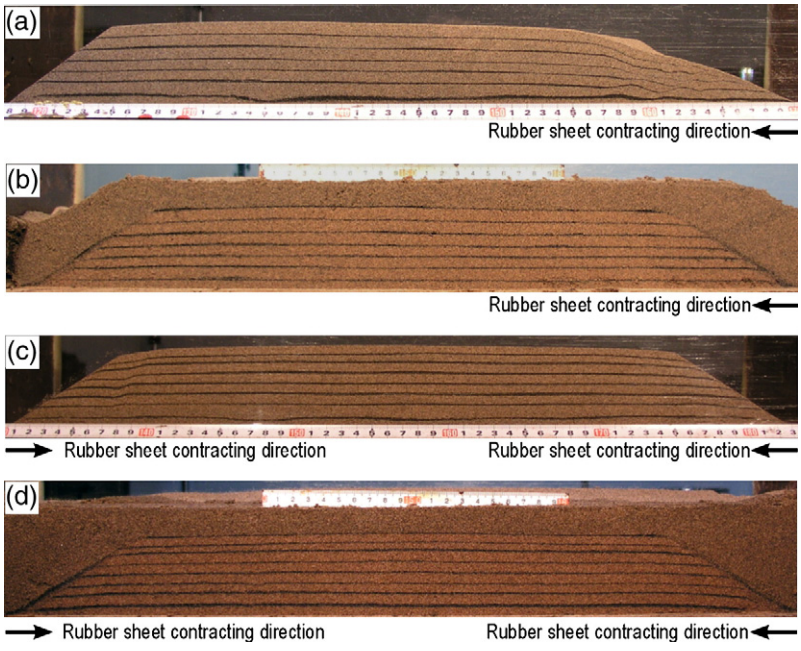

Fig. 10. The photographs of side views and inner sections cut parallel to the substrata contracting direction of the models with contracted substrata but without compression from rear wall, after 15 cm of substrata contraction. (a) Side view and (b) inner section of the model with asymmetrically contracted substratum contracted from one direction at a constant displacement velocity of 4.40×10^{-3} cm/s; (c) side view and (d) inner section of the model with symmetrically contracted substratum contracted simultaneously from two opposite directions both at the constant displacement velocity of 2.20×10^{-3} cm/s.

3.2. Model with anti-directionally contracted substratum

After 13 cm of compression and 13 cm of substratum contraction from the opposite direction, a forward-vergent thrusting wedge of ~17° taper, developed in a frontward sequence, was formed in this model (Fig. 9), which is similar to that of the model above the frictional half of substratum (Fig. 4e, f). However, the sand layers ahead of the thrusting wedge of this model evidently underwent distributed shortening and hunched due to contraction of the substratum (Fig. 9). It is therefore demonstrated that anti-directionally horizontal contraction of ductile substrata can not cause the rearward-vergent thrusting.

3.3. Models with contracted substrata but without compression from rear wall

After 15 cm of substratum contraction from one direction, the side view of the model with asymmetrically contracted substratum exhibits a distributed but apparently asymmetrical deformation style (Fig. 10a). There exist some normal faults by gravitational gliding in the rear domain of the model due to the existence of friction between the sand layers and the glass side wall of sandbox. However, the inner section cut parallel to the substratum contracting direction shows that the inner deformation of the model is also distributed but basically symmetrical with a slight hunch in the central domain (Fig. 10b).

In contrast, the model with symmetrically contracted substratum exhibits symmetrical and distributed deformation both in the side view (Fig. 10c) and the inner section (Fig. 10d), with a slight hunch in the central domain. Only a few normal faults by gravitational gliding exist on the two ends of the model in the side view (Fig. 10c).

Except the frictional conditions between the sand layers and the glass side wall of sandbox, the above two models, whether their substrata were contracted symmetrically or not, have the same kinematical conditions and therefore exhibit identical symmetrical inner deformation styles.

4. Discussion

Results of the physical models aforementioned have demonstrated that only the models with syn-directionally horizontal contraction of substrata (Fig. 6) can reproduce the purely rearward-vergent thrusting wedges. Results of the models with contracted substrata but without compression from rear walls have indicated that horizontal contraction of substrata, whether symmetrically or not, can only produce a distributed and symmetrical deformation style. Results of the model with anti-directionally contracted substratum show that anti-directionally horizontal contraction of ductile substrata can not cause the rearward-vergent thrusting. It is therefore suggested the syn-directionally horizontal contraction of ductile substrata can be an important cause for the formation of purely rearward-vergent (landward-vergent) thrusting wedges, while forward-vergent thrusts are the dominant structures formed above frictional substrata or above ductile substrata undergoing anti-directionally horizontal contraction.

In addition, syn-directionally horizontal contraction of substrata can also reduce the taper of thrusting wedges and promote the propagation of deformation (i.e., larger propagating distance and higher propagating velocity), and therefore result in the almost synchronous deformation and uplift at both the rear and the front of a fold-and-thrust belt with ductile substrata. The plots of uplift versus shortening of the reference points on the surface of the wider half above contractive substrata undergoing syn-directionally horizontal contraction show rough flat-ramp shape (Fig. 7a) and approximate direct proportion between uplift and shortening, indicating that stepwise uplift may be one of the basic features for a fold-and-thrust belt above ductile substrata and for such fold-and-thrust belt the uplift history may roughly reveal its shortening process and vice versa.

4.1. Origin of the purely landward-vergent thrusting wedge along the Cascadia subduction zone

Purely landward-vergent thrusting, an uncommon geological phenomenon, has not been satisfactorily explained by the classical Mohr–Coulomb critical wedge theory and by the relevant numerical models that have successfully explained many other structures in nature (McKay, 1995). A typical purely landward-vergent thrusting wedge exists along the Cascadia subduction zone and its origins has been discussed by many researchers but still remain controversial (e.g. Seely, 1977; McKay et al., 1992; Gutscher et al., 2001; Underwood, 2002). Very low basal friction which may have resulted from ductile substrata and /or excess pore-fluid pressure, a seaward-dipping backstop, a landward dipping decollement and a strong wedge relative to a weak base, have been proposed to be the major probable causes for the formation of a purely landward-vergent thrusting wedge (Byrne and Hibbard, 1987; McKay et al., 1992; Byrne et al., 1993; McKay, 1995; Gutscher et al., 2001; Underwood, 2002). Most of the previous

physical models, with the exception of those of Gutscher et al. (2001), with conditions of low basal friction, seaward-dipping backstop and landward dipping detachment, failed to reproduce purely landward-vergent thrusting domains, but instead produced dual (both searward- and landward-) vergent thrusting domains (e.g. Byrne et al., 1993; Lallemand et al., 1994; Bonini et al., 2000; Smit et al., 2003). On the other hand, based on the results of physical modeling and seismic profile interpretations, Gutscher et al. (2001) ascribed the purely landward-vergent thrusting wedge along the Cascadia subduction zone (from 45°N to 48°N) to the existence of ductile substrata probably composed of calcareous mudstone with excess pore-fluid pressure, but no detailed discussion on the deformation mechanism was given.

The fact that purely rearward-vergent thrusting domains can be successfully reproduced in our physical models, only under the conditions with contractive substrata undergoing syn-directionally horizontal contraction and without forward-dipping backstops and landward dipping detachments, demonstrated that syn-directionally horizontal contraction of ductile substrata can be an important cause for the formation of purely landward-vergent thrusting wedges. Seaward-dipping backstops, landward dipping detachments and strong wedges relative to weak bases are not the necessary requirements, although a seaward-dipping backstop was used in the successful physical models of Gutscher et al. (2001). Seismic profiles from the purely landward-vergent thrusting wedge along the Cascadia subduction zone (see Fig. 2A–C of Gutscher et al. (2001)) evidently show that the substrata gradually thickens landward, suggesting that the substrata may have undergone syn-directionally horizontal contraction by ductile deformation. Furthermore, the ductile substrata composed of silicone putty in the domain of the purely landward-vergent thrusting in the physical model of Gutscher et al. (2001) do not show obvious upward flow (see Figs. 2D and 3 of Gutscher et al. (2001)), also implying that the silicone putty layer may have predominantly undergone syn-directionally horizontal contraction. Accordingly, we can conclude that syn-directionally horizontal contraction of the ductile substrata, which probably consists of calcareous mudstone (Gutscher et al., 2001) or smectite-rich mudstone (Underwood, 2002) with excess pore-fluid pressure, can be an important cause for the formation of the purely landward-vergent thrusting wedge along the Cascadia subduction zone.

It is apparent that the detailed deformation mechanism can not be satisfactorily explained by the classical Mohr–Coulomb critical wedge theory. It is also difficult to clearly explain the deformation mechanism merely based on the results of physical models of ours and Gutscher et al. (2001). We think that further studies by numerical modeling, in combination with physical modeling, may provide effective paths to satisfactorily explain the underlying mechanism. Nevertheless, according to the results of our models, it can be speculated that the syn-directionally horizontal contraction of substrata may have applied a kinematic boundary condition with asymmetric cumulative advection upon the bottom of cover strata, which may produce an effect equivalent to reducing the bottom friction of cover strata in an asymmetric manner and hence promotes the formation of purely landward-vergent thrusting domains. The gradual landward thickening of the ductile substrata underlying the purely landward-vergent thrusting wedge along the Cascadia subduction zone, shown by the seismic profiles (see Fig. 2A–C of Gutscher et al. (2001)), may be one of the natural examples whose ductile substrata have undergone asymmetric cumulative advection.

4.2. Deformation evolution of the Himalayan–Tibetan orogen

The Himalayan–Tibetan orogen, a wide Cenozoic fold-and-thrust belt in central Asia, is characterized by a flat top and steep sides, which was proposed to be closely related to the ductile flow of its weak lower crust (Bird, 1991; Royden et al., 1997; Owens and Zandt, 1997; Clark and Royden, 2000; Shen et al., 2001; Beaumont et al., 2001; DeCelles et al., 2002; Beaumont et al., 2004). Its deformation evolution and uplift history, however, remain controversial.

The surface features of our physical models with syn-directionally contractive substrata are similar to the topography of the Himalayan–Tibetan orogen shown in Fig. 2 of DeCelles et al. (2002). The part of higher-taper forward-vergent thrusting domain in our physical models corresponds roughly to the narrower Himalayan fold-thrust belt, and the part of lower-taper purely rearward-vergent thrusting domain in our physical models, the wider flat-topped Tibetan plateau (compare Fig. 6e with Fig. 2 of DeCelles et al. (2002)). Similar flat-topped surface features were also commonly shown in previous physical models with ductile substrata (e.g. Cotton and Koyi, 2000; Costa and Vendeville, 2002; Lujan et al., 2003; Smit et al., 2003) and in the mechanical and thermal–mechanical models of the Himalayan–Tibetan orogen with weak lower crust (e.g. Royden et al., 1997; Shen et al., 2001; Beaumont et al., 2001, 2004). It is therefore indicated that the

deformation evolution and structural features of the Himalayan–Tibetan orogen may have been governed by its weak lower crust, which probably existed before the deformation of the Himalayan–Tibetan orogen (Clark and Royden, 2000) and may have been further weakened by successive heating and thermal weakening during crustal thickening (Beaumont et al., 2001, 2004).

Many previous physical models with ductile substrata shortened from one side show that the ductile substrata deformed normally in two fashions, asymmetric cumulative advection and flowing upwards (e.g. Cotton and Koyi, 2000; Costa and Vendeville, 2002; Smit et al., 2003; Lujan et al., 2003; Couzens-Schultz et al., 2003; Bonini, 2003). It can be accordingly speculated that the weak lower crust of Himalayan–Tibetan orogen may also have undergone asymmetric cumulative advection by northward indentation of India to produce a syn-directionally contractional basal boundary condition like that in our models with syn-directionally contractive substrata, although currently there are no direct evidences. It is therefore suggested that physical models with syn-directional contractive substrata or ductile substrata may give insights into the deformation evolution of the Himalayan–Tibetan orogen.

There are two different views on the deformation process of the Himalayan–Tibetan orogen. One is that the deformation and uplift in the south and north margin of the Himalayan–Tibetan orogen were almost synchronous, or that the deformation reached the north margin of the Himalayan–Tibetan orogen only 10±5 Ma after the initial collision of India with Asia at 65–55 Ma (e.g. Zhao and Morgan, 1985; Harrison et al., 1992; Molnar et al., 1993; Yin et al., 1999; Yin and Harrison, 2000; Yin et al., 2002; Zhou et al., 2006). The other is that deformation of the Himalayan–Tibetan orogen propagated stepwise northwards, and the deformation and uplift in the north margin of the Himalayan–Tibetan orogen commenced distinctly later than the India–Asia collision (e.g. Tapponnier et al., 1990; Burchfiel et al., 1991; Metivier et al., 1998; Meyer et al., 1998; Tapponnier et al., 2001; Pares et al., 2003). The mechanical or thermal–mechanical models with a weak ductile lower crust but without a distributed contractional basal boundary condition (e.g. Royden et al., 1997; Shen et al., 2001; Beaumont et al., 2001, 2004) generally show northward deformation propagation, which is not well consistent with the increasing geological evidences that support almost synchronous Cenozoic deformation evolution in the north and south edges of the Himalayan–Tibetan orogen (e.g. Yin and Harrison, 2000; Yin et al., 2002; Zhou et al., 2006), although these models well reproduced the flat-topped topography of the Himalayan–Tibetan orogen. In contrast, our physical models with syn-directional contractive substrata (Fig. 6) and the previous physical models with ductile substrata of asymmetric cumulative advection (e.g. Cotton and Koyi, 2000; Costa and Vendeville, 2002; Smit et al., 2003; Lujan et al., 2003) generally exhibited not only the flat-topped topography but also the almost synchronous deformation and uplift at both the rear and front (e.g. Fig. 7), implying that syn-directionally contractional basal boundary conditions may be an important cause for almost synchronous Cenozoic deformation evolution in the north and south edges of the orogen. It is therefore suggested that the north and south edges of the Himalayan–Tibetan orogen may have undergone almost synchronous Cenozoic deformation evolution due to the existence of weak lower crust that may have undergone asymmetric cumulative advection.

Results of physical modeling have well indicated that thrusts in the fold-and-thrust belts above frictional substrata developed dominantly in a frontward sequence (e.g. Fig. 4; Liu et al., 1992). However, thrusts in the fold-and-thrust belts with ductile substrata often developed in a non-frontward sequence, mostly in a synchronous sequence or out-of-sequence and some in a backward sequence (e.g. Fig. 6f; Costa and Vendeville, 2002; Smit et al., 2003). It is therefore suggested that owing to the existence of weak lower crust, development of thrusts in the Himalayan–Tibetan orogen may not necessarily occur in frontward sequence as implied by Tapponnier et al. (2001).

The plots of uplift versus shortening of our physical models with syn-directional contractive substrata (Fig. 7a) have also shown that for a fold-and-thrust belt with ductile substrata, uplift is distinctly slower at its front than at its rear, implying that uplift velocity or elevation thresholds sensible for sedimentation or environment change may have been achieved distinctly later at the northeastern margin of the Himalayan–Tibetan orogen than at its southern parts. Therefore there were probably no sedimentary responses to early long-term weak deformation and uplifting in the northeastern margin of the Himalayan–Tibetan orogen, and the Cenozoic sediments (e.g. Li and Fang, 1999; Pares et al., 2003; Fang et al., 2003; Fang et al., 2005) can only record the much later uplifting of northeastern margin of the Himalayan–Tibetan orogen. Accordingly it is proposed that the much later uplift deduced from Cenozoic sedimentary records in the basins along the northeastern margin of the Himalayan–Tibetan orogen does not necessarily imply much later initiation of uplift

and deformation at the northeastern margin of the orogen as proposed by Tapponnier et al. (2001) and Pares et al. (2003).

5. Conclusions

1. Purely landward-vergent thrusting wedges can be reproduced under the condition of syn-directionally horizontal contraction of ductile substrata without other requirements of seaward-dipping backstops, landward dipping detachments and strong wedges relative to weak bases. Syn-directionally horizontal contraction of ductile substrata, which probably consists of calcareous mudstone or smectite-rich mudstone with excess pore-fluid pressure, can be an important cause for the formation of purely landward-vergent thrusting wedge along the Cascadia subduction zone (from 45°N to 48°N).
2. The results of our physical models with syn-directionally contracted substrata or previous physical models with ductile substrata reinforce the opinion that the deformation evolution and structural features of the Himalayan–Tibetan orogen were likely governed by its weak lower crust and suggest that the north and south edges of the Himalayan–Tibetan orogen may have undergone almost synchronous Cenozoic deformation evolution owing to the existence of weak lower crust that may have undergone asymmetric cumulative advection.
3. It is proposed that development of thrusts in the Himalayan–Tibetan orogen may have not necessarily occurred in a frontward sequence and much later uplift deduced from Cenozoic sedimentary records in the basins along the northeastern margin of the Himalayan–Tibetan orogen does not necessarily imply much later initiation of uplift and deformation at the northeastern margin of the orogen.

Acknowledgments

The authors are grateful to Drs. Yanshao Chen and Qingren Meng for helpful discussions and to Dr. Chris Beaumont for his constructive reviews and helpful suggestions that led to the improvement of the manuscript. This work was supported by Natural Sciences Foundation of China grants (No. 40572112, 40372098).

References

Beaumont, C., Jamieson, R., Nguyen, M., Lee, B., 2001. Himalayan tectonics explained by extrusion of a low-viscosity crustal channel coupled to focused surface denudation. Nature 414, 738–742.

Beaumont, C., Jamieson, R., Nguyen, M., Medvedev, S., 2004. Crustal channel flows: 1. Numerical models with applications to the tectonics of the Himalayan–Tibetan orogen. J. Geophys. Res. 109, B06406. doi:10.1029/2003JB002809.

Bird, P., 1991. Lateral extrusion of lower crust from under high topography in the isostatic limit. J. Geophys. Res. 96 (B6), 10275–10286.

Bonini, M., 2003. Detachment folding, fold amplification, and diapirism in thrust wedge experiments. Tectonics 22, 1065. doi:10.1029/2002TC001458.

Bonini, M., Sokoutis, D., Mulugeta, G., Katrivanos, E., 2000. Modelling hanging wall accommodation above rigid thrust ramps. J. Struct. Geol. 22, 1165–1179.

Burchfiel, B., Zhang, P., Wang, Y., Zhang, W., Song, F., Deng, Q., Molnar, P., Royden, L., 1991. Geology of the Haiyuan fault zone, Ningxia-Hui Autonomous Region, China, and its relation to the evolution of the northeastern margin of the Tibetan plateau. Tectonics 10, 1091–1110.

Burg, J., Davy, P., Martinod, J., 1994. Shortening of analogue models of the continental lithosphere: new hypothesis for the formation of the Tibetan plateau. Tectonics 13, 475–483.

Byrne, T., Hibbard, J., 1987. Landward vergence in accretionary prisms: the role of the backstop and thermal history. Geology 15, 1163–1167.

Byrne, D., Wang, W., Davis, D., 1993. Mechanical role of backstops in the growth of forearcs. Tectonics 12, 123–144.

Chemenda, A., Mattauer, M., Malavieille, J., Bokun, A., 1995. A mechanism for syn-collisional rock exhumation and associated normal faulting: results from physical modeling. Earth Planet. Sci. Lett. 132, 225–232.

Chemenda, A., Burg, J., Mattauer, M., 2000. Evolutionary model of the Himalaya–Tibet system: geopoem based on new modelling, geological and geophysical data. Earth Planet. Sci. Lett. 174, 397–409.

Clark, M., Royden, L., 2000. Topographic ooze: building the eastern margin of Tibet by lower crustal flow. Geology 28, 703–706.

Cobbold, P., Durand, S., Mourgues, R., 2001. Sandbox modelling of thrust wedges with fluid-assisted detachments. Tectonophysics 334, 245–258.

Costa, E., Vendeville, B., 2002. Experimental insights on the geometry and kinematics of fold-and-thrust belts above weak, viscous evaporitic decollement. J. Struct. Geol. 24, 1729–1739.

Cotton, J., Koyi, H., 2000. Modeling of thrust fronts above ductile and frictional detachments: application to structures in the Salt Range and Potwar Plateau, Pakistan. Geol. Soc. Amer. Bull. 112, 351–363.

Couzens-Schultz, B., Vendeville, B., Wiltschko, D., 2003. Duplex style and triangle zone formation: insights from physical modeling. J. Struct. Geol. 25, 1623–1644.

Dahlen, F., 1990. Critical taper model of fold-and-thrust belts and accretionary wedges. Annu. Rev. Earth Planet. Sci. 18, 55–99.

Davis, D., Suppe, J., Dahlen, F., 1983. Mechanics of fold and thrust belts and accretionary wedges. J. Geophys. Res. 88 (B2), 1153–1172.

Davy, P., Cobbold, P., 1991. Experiments on shortening of a 4-layer model of the continental lithosphere. Tectonophysics 188, 1–25.

DeCelles, P., Robinson, D., Zandt, G., 2002. Implications of shortening in the Himalayan fold-thrust belt for uplift of the Tibetan Plateau. Tectonics 21, 1062. doi:10.1029/2001TC001322.

Dubey, A., 1997. Simultaneous development of noncylindrical folds, frontal ramps, and transfer faults in a compressional regime: experimental investigations of Himalayan Examples. Tectonics 16, 336–346.

Fang, X., Garzione, C., Van der Voo, R., Li, J., Fan, M., 2003. Flexural subsidence by 29 Ma on the NE edge of Tibet from the

magnetostratigraphy of Linxia Basin, China. Earth Planet. Sci. Lett. 210, 545–560.
Fang, X., Zhao, Z., Li, J., Yan, M., Pan, B., Song, C., Dai, S., 2005. Magnetostratigraphy of the late Cenozoic Laojunmiao anticline in the northern Qilian Mountains and its implications for the northern Tibetan Plateau uplift. Sci. China, D 48, 1040–1051.
Gutscher, M., Kukowski, N., Malavieille, J., Lallemand, S., 1998. Material transfer in accretionary wedges from analysis of a systematic series of analog experiments. J. Struct. Geol. 20, 407–416.
Gutscher, M., Klaeschen, D., Flueh, E., Malavieille, J., 2001. Non-Coulomb wedges, wrong-way thrusting, and natural hazards in Cascadia. Geology 29, 379–382.
Harrison, T., Copeland, P., Kidd, W., Yin, A., 1992. Raising Tibet. Science 255, 1663–1670.
Koyi, H., Vendeville, B., 2003. The effect of decollement dip on geometry and kinematics of model accretionary wedges. J. Struct. Geol. 25, 1445–1450.
Lallemand, S., Schnurle, P., Malavieille, J., 1994. Coulomb theory applied to accretionary and nonaccretionary wedges: Possible causes for tectonic erosion and/or frontal accretion. J. Geophys. Res. 99 (B6), 12033–12055.
Li, J., Fang, X., 1999. Uplift of the Tibetan Plateau and environmental changes. Chin. Sci. Bull. 44, 2117–2124.
Liu, H., McClay, K., Powell, D., 1992. Physical models of thrust wedges. In: McClay, K. (Ed.), Thrust tectonics. Chapman and Hall, New York, pp. 71–81.
Lohrmann, J., Kukowski, N., Adam, J., Oncken, O., 2003. The impact of analogue material properties on the geometry, kinematics, and dynamics of convergent sand wedges. J. Struct. Geol. 25, 1691–1711.
Lujan, M., Storti, F., Balanya, J., Crespo-Blanc, A., Rossetti, F., 2003. Role of decollement material with different rheological properties in the structure of the Aljibe thrust imbricate (Flysch Trough, Gibraltar Arc): an analogue modelling approach. J. Struct. Geol. 25, 867–881.
Marques, F., Cobbold, P., 2002. Topography as a major factor in the development of arcuate thrust belts: insights from sandbox experiments. Tectonophysics 348, 247–268.
Marques, F., Cobbold, P., 2006. Effects of topography on the curvature of fold-and-thrust belts during shortening of a 2-layer model of continental lithosphere. Tectonophysics 415, 65–80.
McKay, M., 1995. Structural variation and landward vergence at the toe of the Oregon accretionary prism. Tectonics 14, 1309–1320.
McKay, M., Moore, G., Cochrane, G., Moore, J., Kulm, L., 1992. Landward vergence and oblique structural trends in the Oregon margin accretionary prism: implications and effect on fluid flow. Earth Planet. Sci. Lett. 109, 477–491.
Metivier, F., Gaudemer, Y., Tapponnier, P., Meyer, B., 1998. Northeastward growth of the Tibet Plateau deduced from balanced reconstruction of two depositional areas: the Qaidam and Hexi Corridor basins, China. Tectonics 17, 823–842.
Meyer, B., Tapponnier, T., Bourjot, L., Metivier, F., Gaudemer, Y., Peltzer, G., Guo, S., Chen, Z., 1998. Crustal thickening in Gansu–Qinghai, lithospheric mantle subduction, and oblique, strike-slip controlled growth of the Tibet Plateau. Geophys. J. Int. 135, 1–47.
Molnar, P., England, P., Martinod, J., 1993. Mantle dynamics, uplift of the Tibetan Plateau and the Indian monsoon. Rev. Geophys. 31, 357–396.
Mugnier, J., Baby, P., Colletta, B., Vinour, P., Bale, P., Leturmy, P., 1997. Thrust geometry controlled by erosion and sedimentation: a view from analogue models. Geology 25, 427–430.
Owens, T., Zandt, G., 1997. Implications of crustal property variations for models of Tibetan plateau evolution. Nature 387, 37–43.
Pares, J., Van der Voo, R., Downs, W., Yan, M., Fang, X., 2003. Northeastward growth and uplift of the Tibetan Plateau: magnetostratigraphic insights from the Guide Basin. J. Geophys. Res. 108 (B1), 2017. doi:10.1029/2001JB001349.
Peltzer, G., Tapponnier, P., 1988. Formation and evolution of strike–slip faults, rifts, and basins during the India–Asia Collision: an experimental approach. J. Geophys. Res. 93 (B12), 15085–15117.
Persson, K., Sokoutis, D., 2002. Analogue models of orogenic wedges controlled by erosion. Tectonophysics 356, 323–336.
Rossetti, F., Faccenna, C., Ranalli, G., Storti, F., 2000. Convergence rate-dependent growth of experimental viscous orogenic wedges. Earth Planet. Sci. Lett. 178, 367–372.
Rossetti, F., Feccenna, C., Rannalli, G., 2002. The influence of backstop dip and convergence velocity in the growth of viscous doubly-vergent orogenic wedges: insights from thermomechanical laboratory experiments. J. Struct. Geol. 24, 953–962.
Royden, L., Burchfiel, B., King, R., Wang, E., Chen, Z., Shen, F., Liu, Y., 1997. Surface deformation and lower crustal flow in eastern Tibet. Science 276, 788–790.
Seely, D., 1977. The significance of landward vergence and oblique structural trends on trench inner slopes. In: Talwani, M., Pitman, W. (Eds.), Island arcs, deep sea trenches, and back-arc basins: Maurice Ewing Series, vol. 1. American Geophysical Union, Washington, D.C., pp. 187–198.
Shen, F., Royden, L., Burchfiel, B., 2001. Large-scale crustal deformation of the Tibetan Plateau. J. Geophys. Res. 106 (B4), 6793–6816. doi:10.1029/2000JB900389.
Smit, J., Brun, J., Sokoutis, D., 2003. Deformation of brittle-ductile thrust wedges in experiments and nature. J. Geophys. Res. 108 (B10), 2480. doi:10.1029/2002JB002190.
Sokoutis, D., Bonini, M., Medvedev, S., Boccaletti, M., Talbot, C., Koyi, H., 2000. Indentation of a continent with a built-in thickness change: experiment and nature. Tectonophysics 320, 243–270.
Storti, F., McClay, K., 1995. Influence of syntectonic sedimentation on thrust wedges in analogue models. Geology 23, 999–1002.
Tapponnier, P., Peltzer, G., Le Dain, A., Armijo, R., 1982. Propagating extrusion tectonics in Asia: new insights from simple experiments with plasticine. Geology 10, 611–616.
Tapponnier, P., Meyer, B., Avouac, J., Gaudemer, Y., Peltzer, G., Guo, S., Xiang, H., Yin, K., Chen, Z., Cai, S., Dai, H., 1990. Active thrusting and folding in the Qilian Shan, and decoupling between upper crust and mantle in northeastern Tibet. Earth Planet. Sci. Lett. 97, 382–403.
Tapponnier, P., Xu, Z., Roger, F., Meyer, B., Arnaud, N., Wittlinger, G., Yang, J., 2001. Oblique stepwise rise and growth of the Tibet Plateau. Science 294, 1671–1677.
Teixell, A., Koyi, H., 2003. Experimental and field study of the effects of lithological contrasts on thrust-related deformation. Tectonics 22, 9-1–9-18. doi:10.1029/2002TC001407.
Underwood, M., 2002. Strike-parallel variations in clay minerals and fault vergence in the Cascadia subduction zone. Geology 30, 155–158.
Yin, A., Harrison, T., 2000. Geologic evolution of the Himalayan–Tibetan orogen. Annu. Rev. Earth Planet. Sci. 28, 211–280.
Yin, A., Harrison, T., Murphy, M., Grove, M., Nie, S., Ryerson, F., Wang, X., Chen, Z., 1999. Tertiary deformation history of southeastern and southwestern Tibet during the Indo–Asian collision. Geol. Soc. Amer. Bull. 111, 1644–1664.
Yin, A., Rumelhart, P., Butler, R., Cowgill, E., Harrison, T., Foster, D., Zhang, Q., Zhou, X., Wang, X., Hanson, A., Raza, A., 2002. Tectonic history of the Altyn Tagh fault system in northern Tibet inferred from Cenozoic sedimentation. Geol. Soc. Amer. Bull. 114, 1257–1295.

Zhao, W., Morgan, W., 1985. Uplift of Tibetan Plateau. Tectonics 4, 359–369.

Zhao, W., Morgan, W., 1987. Injection of Indian crust into Tibetan lower crust: a two-dimensional finite element model study. Tectonics 6, 489–504.

Zhou, J., Xu, F., Wang, T., Cao, A., Yin, C., 2006. Cenozoic deformation history of the Qaidam Basin, NW China: Results from cross-section restoration and implications for Qinghai–Tibet Plateau tectonics. Earth Planet. Sci. Lett. 243, 195–210.